Huang et al. *NPG Asia Materials* (2023)15:62
https://doi.org/10.1038/s41427-023-00510-y

NPG Asia Materials

ARTICLE Open Access

Triplet-mediated spin entanglement between organic radicals: integrating first principles and open-quantum-system simulations

Tianhong Huang[1,2,3], Jiawei Chang[3], Lin Ma[3], Andrew J. Fisher[4], Nicholas M. Harrison[5], Taoyu Zou[3], Hai Wang[1,3] and Wei Wu[4,6]

Abstract

Controlling molecular spin quantum bits optically offers the potential to effectively reduce decoherence and raise the working temperature of quantum computers. Here, exchange interactions and spin dynamics, as mediated by an optically driven triplet state, are calculated for a molecule that consists of a pair of radicals and represents a potential quantum-circuit building block. Consistent with the previous experimental observation of spin coherence induced by the triplet state, our work demonstrates an optically driven quantum gate operation scheme in a molecule. A technological blueprint combining a two-dimensional molecular network and programmable nanophotonics, both of which are sufficiently developed, is proposed. We thus realize computational exploration of chemical databases to identify suitable candidates for molecular spin quantum bits and couplers to be hybridized with nanophotonic devices. The work presented here is proposed to realize a new approach for exploring molecular excited states and click chemistry, toward advancing molecular quantum technology.

Introduction

The quality of quantum bits (qubits) and the control engineering for quantum gate operations are indispensable aspects of quantum software and related algorithms in quantum computing (QC)[1]. Molecular spin qubits have recently attracted much attention due to their potential not only in high-temperature quantum computing but also in scaling up quantum circuits by chemical synthesis[2–14], which are two important challenges that are yet to be overcome. Addressing individual molecular spins using the combination of electron paramagnetic resonance (EPR) and scanning tunnelling microscopy (STM) has been experimentally demonstrated recently, indicating the unique potential of molecules for QC[14]. Moreover, developing energy-efficient and sustainable quantum technology is a crucial aspect of commercialization, which would be improved by more accessible working conditions such as high-temperature (or even room-temperature) QC[15]. Recent proposals of molecular QC platforms, which explore an optically accessible triplet state to manipulate molecular spin qubits, could shed light on the aforementioned key challenges in QC[16–20]. Computational design and simulations that integrate first principles calculations and open-quantum dynamics are important for the realization of molecular QC networks[7].

A radical molecule containing $\frac{1}{2}$-spins is a natural realization of a qubit[21,22]. An example of an organic radical, 4,4,5,5-tetramethyl-1-yloxyimidazolin-2-yl (TYY), is shown in Fig. 1a. The spin relaxation and coherence times of such organic radicals can be very long (up to seconds) even at high or room temperature due to weak spin-orbit coupling and hyperfine interactions, which is beneficial for applications in QC[2–6]. Mediating the spin–spin

Correspondence: Taoyu Zou (taoyuzou@sina.com) or Hai Wang (haiwang@ynu.edu.cn) or Wei Wu (wei.wu@ucl.ac.uk)
[1]School of Physics and Astronomy, Center for Optoelectronics Engineering Research, Yunnan University, Kunming 650091, P. R. China
[2]School of Physical Science and Technology, Kunming University, Kunming, Yunnan Province, P. R. China
Full list of author information is available at the end of the article

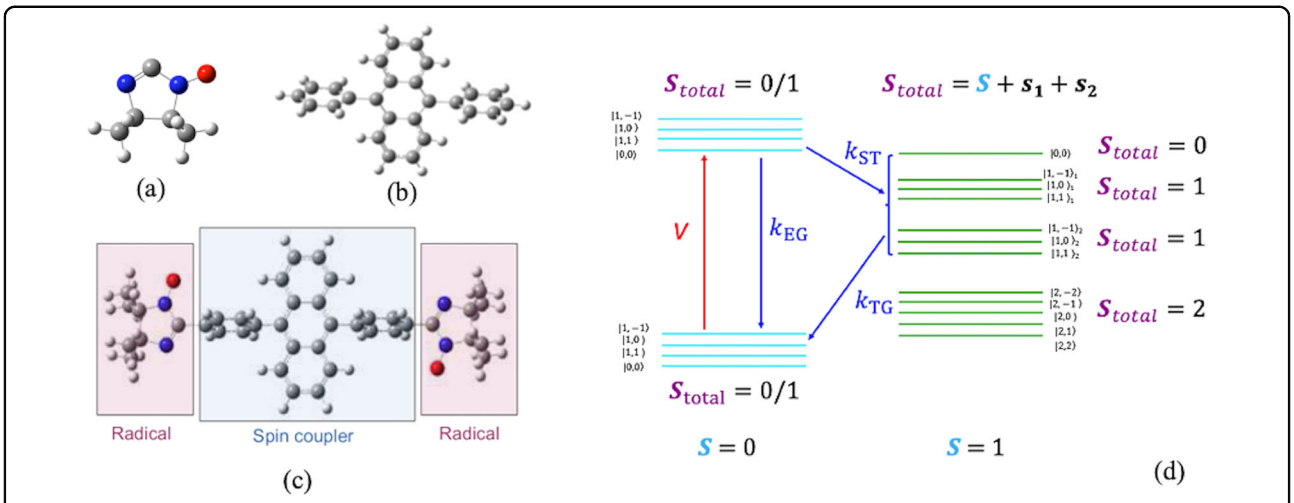

Fig. 1 One example for the biradical systems and the spin coupling mechanism are shown. (**a**) TYY radical, (**b**) DPA spin coupler, and (**c**) combined double-radical triplet system. In (**d**), we have shown the coherent and incoherent processes. The coherent processes include spin–spin interactions among radicals and triplet and optical driving fields (V), while the incoherent processes include intersystem crossing and decays of the triplet and singlet excited states. The decay rates k_{ST}, k_{TG}, and k_{EG} are also illustrated.

interaction between molecular spin qubits has been studied previously based on electronic gating, e.g., using STM tips[23–26]. For multiqubit gate operations, a promising route to control the interaction between spin qubits is optical excitation[16,17]. A molecule consisting of radicals linked by an optically active spin coupler, such as bi4,4,5,5-tetramethyl-1-yloxyimidazolin-2-yl-diphenyl-anthracene (biTYY-DPA), as shown in Fig. 1, could be an ideal platform for quantum gate operation. The di-phenyl anthracene (DPA) molecule, shown in Fig. 1b, can be excited from a singlet ground state to a triplet state via intersystem crossing (ISC)[27], thus mediating the interaction among radicals in biTYY-DPA (Fig. 1c). The ISC process is normally very fast (e.g., nanoseconds), whereas the lifetime of the triplet, characterized by the parameter k_{tg}^{-1} (k_{tg} being the decay rate from the triplet to the singlet ground state), is usually long (e.g., milliseconds) because the decay to the singlet ground state is forbidden due to spin momentum conservation and hence dominated by nonradiactive processes. This spin coupling mechanism offers a promising route to control quantum gate operations at a time scale of ~nanoseconds and is shown in Fig. 1d. Before optical excitation, the two spin-$\frac{1}{2}$ radicals form a singlet and triplet, i.e., $\frac{1}{2} \otimes \frac{1}{2} = 0 \oplus 1$, which also applies when there is singlet excitation on the spin coupler. After optical excitation and ISC, the triplet (spin-1) is coupled with two doublets, i.e., $1 \otimes \frac{1}{2} \otimes \frac{1}{2} = 2 \oplus 1 \oplus 1 \oplus 0$ (one quartet, two triplets, and one singlet). The four spin manifolds are shown in Fig. 1d; here, we assume that the coupling between them is ferromagnetic (FM, the $S = 2$ state is the lowest manifold).

Extensive experimental efforts combining time-resolved EPR (TREPR) and optical excitations[14,28–32] have been reported to control exchange interactions in biradicals, such as biTYY-DPA (Fig. 1c). Most TREPR experiments can be performed at high temperature (77 K, the boiling point of liquid nitrogen), which could facilitate the development of more practical quantum technologies. Previously, a first-principles calculation was carried out for the spin-2 state of the biTYY-DPA molecule, and a qualitative model for the spin dynamics in biradicals was proposed[33]. In addition, nuclear spins have been coupled through triplet excitation of C_{60}, inspiring us to explore radical electron spins for faster quantum-gate response[16]. To the best of the authors' knowledge, there have been few reports (i) considering quantitative calculation of the exchange interaction between the transient triplet and radicals and (ii) demonstrating simulations of the TREPR spectra using the theory of open quantum systems[34], both of which are explored here. Our theoretical findings provide a theoretical foundation for realizing a promising route to assemble molecules for quantum circuits. Our theoretical calculation results are in good agreement with the previous experimental results. In particular, we have proposed a molecular architecture integrated with nano-photonic devices to scale up and control quantum circuits, thus potentially demonstrating an advancement toward large-scale optically driven molecular quantum computing.

Methods

First-principles density-functional-theory calculations for exchange interactions

First-principles calculations were carried out using hybrid exchange density function theory (HDFT) with a 6–31 G basis set in the Gaussian 09 code[35]. The self-

consistent field (SCF) procedure converged to a tolerance of 10^{-6} a.u. (~0.3 Kelvin). The broken-symmetry method[36] was used to allow spins to localize on the radicals and the convergence to a low-spin configuration. Electronic exchange and correlation are described using the B3LYP hybrid exchange density functional[37], the advantages of which include a partial elimination of the electronic self-interaction error and a balance of the tendencies to delocalize one-electron wave functions. The B3LYP density functional has previously been shown to provide an accurate description of the electronic structure and magnetic properties of organic compounds[38,39].

Supposing we have two radicals and one spin coupler and the exchange interaction dominates over both dipolar interactions and spin-orbit coupling, then the Heisenberg spin Hamiltonian before optical excitations reads

$$\hat{H}_0 = J_0 \hat{\vec{s}}_1 \cdot \hat{\vec{s}}_2, \tag{1}$$

where J_0 is the exchange interaction between radical spins $\hat{\vec{s}}_1$ and $\hat{\vec{s}}_2$, which can be computed as the energy difference between the triplet and broken-symmetry (BS) states of radicals, $J_0 = 2(E_{\text{triplet}} - E_{\text{BS}})$. When the spin coupler is in a triplet state after optical excitations, the spin Hamiltonian therefore changes to

$$\hat{H}_1 = J_1 \hat{\vec{s}}_1 \cdot \hat{\vec{S}} + J_2 \hat{\vec{S}} \cdot \hat{\vec{s}}_2 + J_3 \hat{\vec{s}}_1 \cdot \hat{\vec{s}}_2, \tag{2}$$

where J_1 (J_2) is defined as the exchange interaction between radical spins $\hat{\vec{s}}_1$ ($\hat{\vec{s}}_2$) and the triplet spin $\hat{\vec{S}}$. J_3 is the exchange interaction between two radical spins after optical excitations. To compute J_1, J_2, and J_3, we first find the total energies of the states $|a\rangle = |\uparrow\Uparrow\uparrow\rangle$, $|b\rangle = |\uparrow\Uparrow\downarrow\rangle$, $|c\rangle = |\downarrow\Uparrow\downarrow\rangle$, and $|d\rangle = |\downarrow\Uparrow\uparrow\rangle$, where $\uparrow(\downarrow)$ is defined as the spin state $|s = \frac{1}{2}, s_z = \frac{1}{2}(|s = \frac{1}{2}, s_z = -\frac{1}{2})$ of a radical and $\Uparrow$ as $|S = 1,\ S_z = 1\rangle$ for the spin-coupler triplet. Then, we obtain

$$\begin{aligned} J_1 &= (\Delta E_{ac} + \Delta E_{bd})/2, \\ J_2 &= (\Delta E_{ac} - \Delta E_{bd})/2, \\ J_3 &= \Delta E_{ab} + \Delta E_{cd}, \end{aligned} \tag{3}$$

where $\Delta E_{ij} = E_i - E_j$ is defined as the energy difference between the states with spin configurations i and j ($\in \{a,b,c,d\}$).

Note that the broken-symmetry singlet and triplet states formed by two radical spins alone have the same spin z-component as $|b\rangle$ and $|c\rangle, |d\rangle$, respectively, but much lower energies, owing to the triplet excitation energy (~ eV in general). The Kohn-Sham orbitals therefore need to be repopulated to drive the system into $|b\rangle$, $|c\rangle$, or $|d\rangle$. If two radicals are symmetric, then $E_b = E_d$ and therefore

$$\begin{aligned} J_1 &= J_2 = \Delta E_{ac}/2, \\ J_3 &= \Delta E_{ab} + \Delta E_{cb}. \end{aligned} \tag{4}$$

The expectation value of the squared total spin operator $\hat{\vec{S}}^2_{total} = (\hat{\vec{s}}_1 + \hat{\vec{S}} + \hat{\vec{s}}_2)^2$ is 6 for the state $|a\rangle$ (since it is a total spin eigenstate with $S_{\text{total}} = 2$), 3 for $|b\rangle$ and $|d\rangle$, and 2 for $|c\rangle$. We adopted that the exchange interactions are anti-ferromagnetic (AFM) when $J > 0$, while they are FM when $J < 0$. The spin Hamiltonians in Eq. 1 and Eq. 2 and the computation of the exchange interactions therein can be generalized to the molecular structure with more radicals.

Above, J_1 is equal to J_2 because the biTYY-DPA molecule has an inversion symmetry. J_0, J_1, and J_3 were computed for the dihedral angles between the phenyl ring and the anthracene, ranging from 0° (coplanar) to 90° (perpendicular) with 10° increments. In all the calculations, we froze the TYY radicals and rotated only the phenyl ring, which meant that we assumed that the dihedral angles at each end of the coupler were equal.

The time evolution of the density matrix and TR-EPR spectra simulations

System Hamiltonian

After considering the optical driving field, the total Hamiltonian is updated to

$$\begin{aligned} \hat{H}_{opt} = {} & |S_0\rangle[\hat{H}_0 + g_r\mu_B \overrightarrow{B} \cdot (\widehat{\vec{s}}_1 + \widehat{\vec{s}}_2)]\langle S_0| \\ & + |S_1\rangle[\hat{H}_0 + g_r\mu_B \overrightarrow{B} \cdot (\widehat{\vec{s}}_1 + \widehat{\vec{s}}_2)]\langle S_1| \\ & + |T_1\rangle[\hat{H}_1 + g_r\mu_B \overrightarrow{B} \cdot (\widehat{\vec{s}}_1 + \widehat{\vec{s}}_2) \\ & + g_c\mu_B \overrightarrow{B} \cdot \widehat{\vec{S}} + D\hat{S}_z^2 + E(\hat{S}_x^2 - \hat{S}_y^2)]\langle T_1| \\ & + V(|S_0\rangle\langle S_1| + |S_1\rangle\langle S_0|). \end{aligned} \tag{5}$$

where, S_0 is the singlet ground state of the spin coupler, S_1 is the first singlet excited state, and T_1 is the triplet ground state. D and E are the zero-field splittings (ZFS) for the triplet. g_r is the g-factor for the radical spin, while g_c is the g-factor for the coupler spin. V is the transition matrix element between the ground and excited singlet states (S_0 and S_1) due to the optical driving field. $\vec{B}$ is a static magnetic field, and μ_B is the Bohr magneton. $\hat{H}_0$ and $\hat{H}_1$ are defined in Eqs. 1 and 2, respectively. Here, we assume that the exchange interaction between radicals J_0 is unchanged in the singlet excited states.

Quantum jump operators due to system-environment couplings

To include the environmental effects on the time evolution of the density matrix, we used the super operators

(the Liuvillian) within the Markovian approximation, leading to the Lindblad formalism. These super operators are given as

$$\hat{\hat{L}}_i\hat{\rho} = \sum_{\mu=1}^{n_i} \gamma_i^{\mu}\left[\hat{l}_i^{\mu}\hat{\rho}\hat{l}_i^{\mu\dagger} - \frac{1}{2}\{\hat{\rho}, \hat{l}_i^{\mu\dagger}\hat{l}_i^{\mu}\}\right] \tag{6}$$

where, $\hat{\rho}$ is the density matrix for biradicals. The incoherent processes are described by γ_i^{μ} (the decoherence rate) and $\hat{l}_i^{\mu}$ (the quantum jump operator), where i labels different decoherence processes and μ labels the operators in the process. In addition, n_i is the number of operators in each physical process i. For our system, $i = 1$ to 5. $\hat{\hat{L}}_{1,2}$ with $n_{1,2} = 3$ is used to describe the relaxation of the radical spins $\vec{s}_1$ and $\vec{s}_2$ as follows: $\hat{l}_1^{1,2} = \hat{s}_{1,2}^{-}$(spin-$\frac{1}{2}$ lowering operator), $\hat{l}_1^{1,2} = \hat{s}_{1,2}^{+}$ (spin-$\frac{1}{2}$ raising operator), and $\hat{l}_3^{1,2} = \hat{s}_{1,2}^{z}$(the z-component of the spin-$\frac{1}{2}$). The $\hat{s}^z$ operator is responsible for the pure dephasing of quantum states, wherea $\hat{s}^+$ and $\hat{s}^-$ for quantum jumps. $\hat{\hat{L}}_2$ with $n_2 = 8$ is used as a super operator to describe the relaxation of the triplet state. We used the corresponding eight Gell-Mann matrices for these operators. Moreover, we take into account the spin–spin (transverse spin) relaxation[40] within the mean-field approximation induced by the interaction between the spins in the system and those in the environment, i.e., $\hat{s}_1\hat{s}_2 \sim \langle\hat{s}_1\rangle\hat{s}_2$. Hence, the T_2 relaxation processes can be absorbed into the Lindblad formalism $\hat{\hat{L}}_{1,2}$ described above.

In this formulation, we have considered the ISC in$\hat{\hat{L}}_3$ based on assuming that the total spin angular momentum and its z-component are both conserved, i.e., $S_{\text{total}} = 0$ or 1 (twice), thus obtaining the following operators. $\hat{\hat{L}}_3$ with $n_3 = 7$ describes the transitions from the single excited state to the triplet state. For example, some of the operators read $\hat{l}_3^1 = |0,0\rangle_{T_1}\langle 0,0|_{S_1}$ and $\hat{l}_3^2 = |1,-1\rangle_T^1\langle 1,-1|_{S_1}$. Here, we use $|S_{\text{total}}, S_{\text{total},z}\rangle$ to represent our states formed in the triplet (T_1) and the S_1 manifolds, as shown in Fig. 1(d). Similarly, we can define the decay operator $\hat{\hat{L}}_4$ ($n_4 = 7$) for the transition from the triplet state to the singlet ground state. For example, some of the operators read $\hat{l}_4^1 = |0,0\rangle_{S_0}\langle 0,0|_T$ and $\hat{l}_4^2 = |1,-1\rangle_{S_0}\langle 1,-1|_T$. The fifth superoperator $\hat{\hat{L}}_5$ is responsible for the spontaneous decay of the singlet excited state (S_1) down to the ground state (S_0). There are four operators ($n_5 = 4$), including $\hat{l}_5^1 = |0,0\rangle_{S_0}\langle 0,0|_{S_1}$, $\hat{l}_5^2 = |1,-1\rangle_{S_0}\langle 1,-1|_{S_1}$, $\hat{l}_5^3 = |1,0\rangle_{S_0}\langle 1,0|_{S_1}$, and $\hat{l}_5^4 = |1,1\rangle_{S_0}\langle 1,1|_{S_1}$. All the coupling parameters γ_i^{μ}(i from 1 to 5) have been simplified by using a single parameter $\gamma_1^i = \gamma_{\text{radical}}$, $\gamma_2^i = \gamma_{\text{triplet}}$,$\gamma_3^i = k_{st}$, $\gamma_4^i = k_{tg}$, and $\gamma_5^i = k_{eg}$ for these five incoherent processes. In our simulations, we set $\gamma_{\text{radical}} = 0.1$ mT, $\gamma_{\text{triplet}} = 0.1$ mT, $k_{st} = 10$ mT, $k_{tg} = 0.0001$ mT, and $k_{eg} = 10$ mT. The optical driving field is set to be 10 mT. The relaxation times for the spins are ~ 0.1 μs, the ISC rate is on the order of *ns*, and the decay rate for the triplet to the singlet ground state is on the order of *μ*s. All the *g*-factors are set to 2.

The total Liuvillian and the simulation of TREPR spectra

Therefore, the total Liuvillian operator is described as follows

$$\frac{d\hat{\rho}}{dt} = \hat{\hat{\mathcal{L}}}\hat{\rho} = -i[\hat{H}_{opt}, \hat{\rho}] + \left[\sum_{i=1}^{5}\hat{\hat{L}}_i\right]\hat{\rho} \tag{7}$$

where, the first part is the coherent interaction from the effective spin Hamiltonian and optical field (see Eq. 5), which is the commutator between the Hamiltonian and the density matrix. The second part includes the incoherent processes associated with relaxations and crossovers between states (see Eq. 6). Therefore, we have a 20 by 20 Hamiltonian matrix (4 for the singlet ground and excited states with radicals each, 12 for the triplet ground states with radicals), leading to a 400 by 400 Liuvillian.

The TR-EPR spectra is computed as follows[41,42]

$$I_0(t,\omega,\theta,\phi) = |\mathrm{Tr}\{\hat{\rho}(t)S_x^{\text{total}}(\theta,\phi)[i\hat{\hat{\mathcal{L}}}(\theta,\phi) - \omega I]^{-1}S_x^{\text{total}}(\theta,\phi)\}|. \tag{8}$$

where, $S_{\text{mw}}^{\text{total}} = \vec{S}^{\text{total}}\cdot\vec{e}_{mw}$, where $\vec{e}_{mw} = (-\sin\phi, \cos\phi, 0)$, is the total spin component along the microwave field direction, which is always perpendicular to the static magnetic field along the $\vec{e}_{static} = (\sin\theta\cos\phi, \sin\theta\sin\phi, \cos\theta)$ direction, and ω is the microwave field frequency.

We have also computed the powder-averaged TREPR spectra to compare our calculations with the experiments in which molecules are randomly oriented[28], with the relevant equation as follows

$$I(t,\omega) = \int_0^{\pi} d\theta \int_0^{2\pi} d\phi I_0(t,\omega,\theta,\phi). \tag{9}$$

Numerically, we use 50 points uniformly along θ and 100 points uniformly along ϕ (5000 points in total), following the procedure of Easyspin[43].

Results and Discussion

DFT calculations for exchange interactions

When the spin coupler is in its ground state, the two TYY radicals interact weakly through spin polarization (induced by the radical spin) on the coupler. After optical

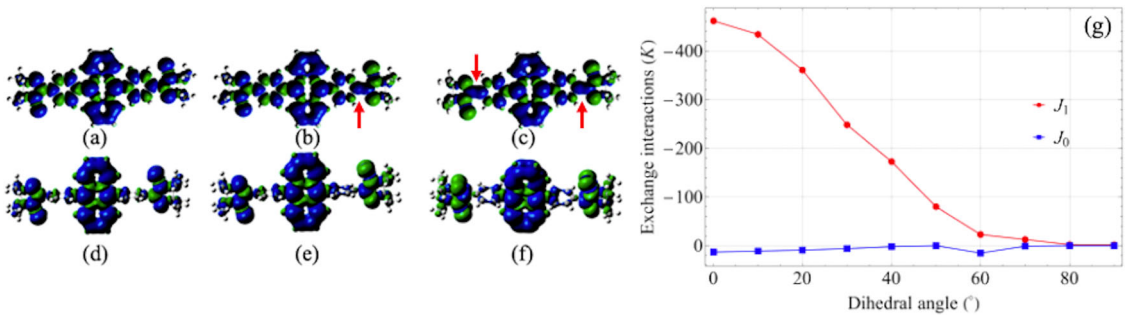

Fig. 2 The computed spin densities and exchange interactions for biTYY-DPA are shown. The isosurfaces of spin densities in biTYY-DPA with a dihedral angle of 0° (90°) with spin configurations $|a\rangle$, $|b\rangle$, and $|c\rangle$ are shown in (**a**–**c**) (**d**–**f**). Positive is in blue, and negative is in green. The isosurface value is set to 0.01e/Å^3. In (g), the exchange interactions J_0 (blue squares) and J_1 (red circles) are plotted as functions of the dihedral angle between the anthracene and the phenyl ring. Notice that for all the angles studied here, the sign of the exchange interaction is switched by optical excitation and ISC and that J_1 decreases as the dihedral angle increases owing to the suppression of the triplet wave function on DPA. On the other hand, the dependence of J_0 on the dihedral angle is more complicated because the exchange interaction between radicals occurs through spin polarization.

excitation and ISC, spin polarization on the coupler is mostly dominated by the triplet spin, as shown in Fig. 2a–f. In our calculations, J_3 is three to four orders smaller than J_0 for all the dihedral angles studied (Fig. 2g). We therefore neglect J_3 in the following. When the dihedral angle is 0°, J_0/k_B is predicted to be 16.8 K and J_1/k_B to be −461.4 K, which is above room temperature. When the dihedral angle is 60°, which is a geometry that has been observed in the DPA crystal structure[44], J_0/k_B is predicted to be 15.2 K and J_1/k_B to be −22.8 K. When the dihedral angle is 90°, J_0 is computed to be negligible; however, the dipolar interaction between the spins is estimated to be $\sim 10^{-4}$ K as the distance between radicals is ~ 17 Å, and J_1/k_B is predicted to be −2.0 K. The calculation results are consistent with the TREPR experiments for the optically driven transient magnetic properties of biTYY-DPA, which confirms that the radical spins are aligned after optical excitation, as shown in the previous experiment[28]. At suitable temperatures, optical excitation and ISC can change the spin alignment of radicals from AFM to FM with enhanced magnitude. This indicates that biTYY-DPA not only has potential for quantum gate operations but can also serve as an optically controlled single-molecule magnetic switch. This structure can potentially function at room temperature if the molecule can be prepared with a dihedral angle smaller than 20° on a surface, as suggested in Fig. 2g. The calculated spin densities reveal the nature of the exchange interactions between the radicals and the triplet on DPA. The spin densities of the three spin configurations $|a\rangle$, $|b\rangle$, and $|c\rangle$ for the dihedral angle of 0° (90°) are shown in Fig. 2a–c, d–f. J_1 decreases as the dihedral angle is increased because the rotation of the phenyl ring away from the coplanar geometry suppresses the delocalization of the $\pi-$orbitals of DPA, which dominate the wave function of the triplet exciton. This dynamic is manifested by the much smaller spin densities on phenyl rings with dihedral angles equal to 90° than 0°, as shown in Fig. 2d–f. The effect of phenyl rings on spin densities implies that we could engineer molecules to control spin densities and thus interaction strength. In contrast to these large variations on the phenyl rings, the spin densities on the radicals are insensitive to the dihedral angle: Mulliken population analysis yields a spin moment of ~0.3 μ_B on the nitrogen and ~0.5 μ_B on the oxygen for all the dihedral angles, which indicates that the radical spins are well preserved despite maintaining an optical excitation on the spin coupler.

The mechanism for the strong radical-triplet exchange interaction J_1 can be described using Ovchinnikov's topological spin alternation rule for π-conjugated systems[45,46]: the spin-up and spin-down densities alternate on the neighboring carbon atoms. The underlying physics of this rule is related to the formation of spin polarization induced by electron delocalization in a π-conjugated system, similar to the indirect exchange mechanism in inorganic insulators[47] and Lieb's theorem for the bipartite graphene lattice[46]. In the $|a\rangle$ state, the spin densities are consistent with Ovchinnikov's topological spin alternation rule, whereas in the $|b\rangle$ and $|c\rangle$ states, the spin alternation pattern is violated when the spin-up densities meet at the junction between the phenyl ring and the TYY radicals (highlighted by the red arrows in Fig. 2b, c). Therefore, the spin-aligned state $|a\rangle$ is favored, and the exchange interaction for the triplet excited state on DPA is FM. This mechanism based on Ovchinnikov's rule could be used to engineer the sign and even the magnitude of the exchange interaction, thus facilitating the design of molecular quantum circuits.

Spin dynamics with optical excitations and TREPR spectra simulations

We have further computed the dynamics of the whole system based on the theory of open quantum systems

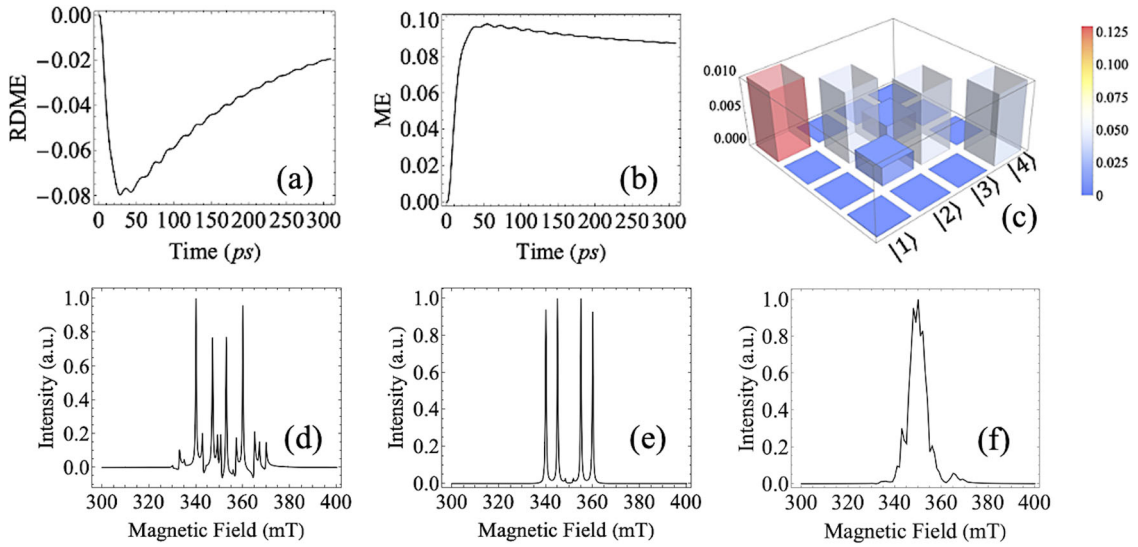

Fig. 3 The time evolutions of the density matrix elements are shown. In **a**, we show the off-diagonal term ($|\frac{1}{2},\frac{1}{2}\rangle\langle\frac{1}{2},-\frac{1}{2}|$) of the reduced density matrix element (RDME) for two radicals, which indicates the entanglement between two radicals created during this process. In **b**, we show the populations for the state $|\frac{1}{2},1,-\frac{1}{2}\rangle$, which has Rabi oscillation behavior. In **c**, we computed the magnitudes of the reduced density matrix for two radicals as tomography. Note that we only plotted up to 0.01. We show the EPR spectra at an early stage with different exchange interactions between radicals and triplets: **d** $J_1 = -10$ mT and (**e**) -10^3 mT for a fixed static magnetic field orientation with $\theta = 0°$ and $\phi = 0°$ (perpendicular to the molecular plane). In **f**, powder-averaging spectra for $J_1 = -10$ mT are shown.

described in §II B. In Fig. 3a, we show the time evolution of the off-diagonal term (coherence) for the reduced density matrix of the two radicals ($|\frac{1}{2},\frac{1}{2}\frac{1}{2},-\frac{1}{2}|$) after tracing out the triplet manifold. We observe that the magnitude of the matrix element will increase when applying the optical driving field and then decays slowly as the triplet vanishes. This result supports that the exchange interaction between radical and triplet induced will trigger coherence or entanglement between the two radical spins. The diagonal term (population) for the $|\frac{1}{2},1,-\frac{1}{2}$ state in the density matrix (Fig. 3b) shows decaying Rabi oscillation characteristics, indicating the coherence created during this process. In Fig. 3c, the tomography for the magnitudes of the reduced density matrix of the two radicals at the early stage ($T = 6.2\,ps$) of the time evolution after applying the optical excitation has been plotted, in which we can clearly see the nonzero off-diagonal term for spin coherence. Here, $|1\rangle = |\frac{1}{2},\frac{1}{2}_L|\frac{1}{2},\frac{1}{2}_R$, $|2\rangle = |\frac{1}{2},\frac{1}{2}_L|\frac{1}{2},-\frac{1}{2}_R$, $|3\rangle = |\frac{1}{2},-\frac{1}{2}_L|\frac{1}{2},\frac{1}{2}_R$, and $|4\rangle = |\frac{1}{2},-\frac{1}{2}_L|\frac{1}{2},-\frac{1}{2}_R$ (L and R label the radical on the left and right, respectively). We also investigated the TREPR spectra at the early stage ($T = 6.2\,ps$) in Fig. 3d–f. We used different parameters for the exchange interaction between radical and triplet, which are comparable to the range of the exchange interactions computed by DFT, as shown in §III A. The exchange interaction between triplet and radical is -10 and -10^3 mT for Fig. 3d and e, respectively. We also computed the powder-averaged spectra, as shown in Fig. 3f. The main and side peaks have successfully been reproduced based on our open-quantum-system modeling compared with the experimental results[28]. Notably, we have not distinguished emission and absorption. For the static magnetic field (X-band), spin anisotropy, spin relaxation rates, ISC rate, and spontaneous decay rate, we used the same parameters as in the previous work[17]. When the exchange interaction is smaller than the static magnetic field (~350 mT), there are more features in the spectra than those from the much larger exchange interaction. The side peaks stem from the triplet state of DPA, while the central peaks (when the exchange interaction is -10 mT) originate from the radical spins, which are renormalized by the interactions with the triplet on DPA. The EPR spectra for the larger exchange interactions are saturated due to the limitation of the magnitude of the static magnetic field, which indicates that the EPR spectra will be dominated by the exchange interaction between the radicals and the triplet. Therefore, in this range of static magnetic fields, we only observe the effect based on the spin anisotropy (D and E). Other instruments are needed to probe the large exchange interaction, such as inelastic neutron scattering[48].

Prediction of the fidelity of the $\sqrt{\mathrm{SWAP}}$ quantum gate operation

To validate the effectiveness of the quantum gate operations based on our aforementioned design, we

performed calculations for the fidelities of $\sqrt{\mathrm{SWAP}}$ quantum gate operations as a function of the T_1 decay rate[23]. The $\sqrt{SWAP}$ quantum gate is defined as $|\alpha,\beta\rangle \rightarrow \frac{|\alpha,\beta\rangle+i|\beta,\alpha\rangle}{1+i}(\alpha,\beta=\uparrow,\downarrow)$. We start from the Hamiltonian shown in Eq. 2 of §II. Here, we neglected J_3 and the ZFS terms if assuming the exchange interactions are dominant; then, this Hamiltonian is determined as follows

$$\hat{H}_2 = -J_1\hat{\vec{S}}_1 \cdot \hat{\vec{S}}_2 + \frac{J_1}{2}\hat{\vec{S}}^2_{\mathrm{total}} \tag{10}$$

where we neglect the constant terms due to S_1^2, S_2^2, and S^2. Then, we observe that $\hat{\vec{S}}^2_{\mathrm{total}}$ can be approximated as a constant of 6 and thus neglected if J_1 is dominant in the spin Hamiltonian such that the system stays in the $S_{\mathrm{total}}=2$ manifold. Thus, we define $\hat{H}_2 \simeq -J_1\vec{S}_1 \cdot \vec{S}_2$, which can then be used to realize the $\sqrt{\mathrm{SWAP}}$ quantum gate under the condition $J_1\tau_{\mathrm{gate}} = \frac{\pi}{2} + 2n\pi$. As J_1 is negative, we set $n=-1$ to maximize the number of quantum gate operations. Here, we assume that the relaxation rate γ of the radical is < 0.1 mT (~ms), which is at least two orders lower than the exchange interaction J_1 here (>10 mK). Then, we can determine the density matrices resulting from the ideal gate (ρ_{ideal}) and that with the environmental effect (ρ_{real}), which are used to compute the fidelity $\mathrm{Tr}[\rho_{\mathrm{real}}\rho_{\mathrm{ideal}}]$, as a function of the ratio between $-J_1$ and $\frac{}{\gamma}$ (Fig. 4). The calculations shown in Fig. 4 indicates that the fidelity of the $\sqrt{\mathrm{SWAP}}$ quantum gate is > 91%, which could be beneficial for this molecule-based quantum gate operation. The other parameters, such as zero-field splitting, might have a minor effect on the gate operation, as the exchange interaction J_1 is dominant even in the worst scenario (the dihedral angle is $^{90^\circ}$). Nevertheless, their effects could be studied in detail in the near future.

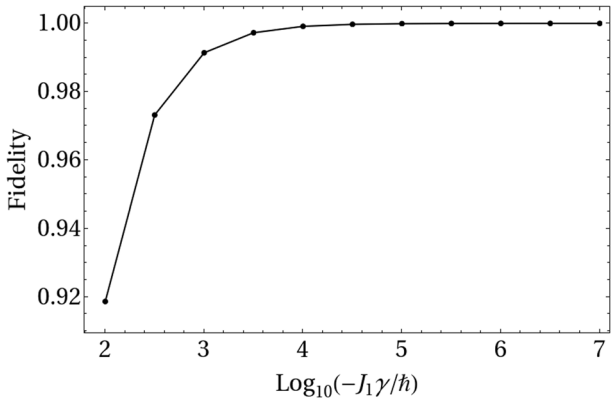

Fig. 4 The fidelity of the $\sqrt{\mathrm{SWAP}}$ quantum gate operation has been computed as a function of the ratio between J_1 and $\frac{}{\gamma}$, where γ is the T_1 decay rate of radical spin-$\frac{1}{2}$. As we can see from the figure, the fidelity can be higher than 91% when $\hbar/\gamma$ is ~2 orders of magnitude lower than the exchange coupling J_1, which is the case in our paper.

QCAD based on molecules

Quantum computer-aided design (QCAD) has recently been proposed for supporting quantum computing architectures based on silicon quantum dots[49–51], which has great potential to optimize quantum circuit design, thus improving design efficiency (although this approach is still in its infancy). Simultaneously, research on two-dimensional (2D) materials has surged rapidly[52–54]. We therefore generalize biradicals to a tentative blueprint for molecular quantum-circuit architecture, as shown in Fig. 5. A molecular two-qubit quantum gate has been proposed and realized in the previous work reported in Ref. [23–26]. A two-qubit quantum gate $\sqrt{\mathrm{SWAP}}$ mediated by electrons controlled by an STM tip using the polyoxometalate molecule has been proposed[23]. Similarly, a two-qubit quantum gate $\sqrt{i\mathrm{SWAP}}$ using two single-molecule Cr7Ni magnets is linked by a redox-active moiety[24]. Nuclear spins with electrical control, leading to a long coherence time, have also been proposed for quantum simulation schemes[25]. Two HoW_{10} molecular qubits have been entangled electrically[26]. These research works are encouraging for the further design of molecular quantum-gate networks. A two-dimensional molecular network consists of radicals (qubits) and a spin coupler, which can ideally be chemically bonded by suitable bridging molecular structures. To assemble optimal radicals and couplers for quantum circuits, 'click chemistry', which has been extremely successful in biochemistry and drug discovery, could provide us with a superior methodology[55]. Atop this molecular network, we could build nanophotonic devices controlling the electronic states of the spin coupler and thus the spins of radicals. The fabrication of optical devices for entanglement control has been demonstrated recently by using an optical twizzer[56]. Moreover, we explore the triplet excited states, i.e., promoting the triplet from the ground state to the excited state, which is expected to allow us to further separate the radicals, ideally tens of nanometer distances, thus easing the design and fabrication of optical devices. We could not only take advantage of the recent development of programmable photonic quantum circuits[57] but also integrate spin qubits with photonics[58]. Regarding the feasibility of fabricating optical devices, one choice is to use recently developed nanometer-size single photon emitters, such as gold tips or nanoscale gaps on WSe_2[59–61]. In addition, quantum calligraphy, in which strains are encoded into 2D materials, can be used to create and locate single-photon emitters with a precision of nanometers[62]. Additionally, nanometer-sized single photon emitters can be fabricated by using quantum dots[63]. Another alternative for optical devices is to use

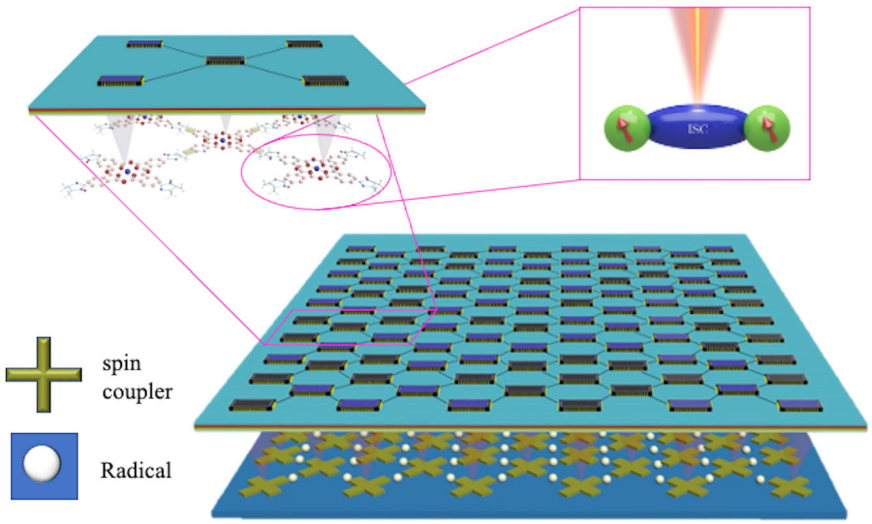

Fig. 5 A QC architecture based on molecules and optical instruments is shown as an illustration of a more complex molecular QC network. The fundamental physical mechanism is coupling radicals through optical excitation and ISC. Here, radicals (TYY as an example) are linked by spin couplers (phthalocyanine molecules as an example), which could be either achieved by van der Waals forces or through chemical bonds by designing bridging molecular structures. The optical devices working as the control unit need to be integrated with the molecular spin couplers, such that we can program them as needed to control quantum gate operation.

organic molecules such as phthalocyanine and dibenzoterrylene that have very good optical emission properties[27,64], which is also compatible with spin couplers, thus further easing integration with the molecular network. As shown in the above sections, the mediating couplings and quantum dynamics have been calculated, which suggests that this proposal is theoretically feasible. The persistence of the exchange interaction between the radical and the triplet could be problematic for read-out. Further work will therefore be needed either to identify mechanisms that can turn off the interaction after a defined time to read out quantum information or to understand how to exploit the always-on interaction to perform quantum computation[65]. In addition, quantum algorithms based on molecular qu*b*it has been proposed, further illustrating the great potential of molecules for QC[4].

Conclusions

In this work, we computed the exchange interactions between radicals and optically induced triplets in a biradical molecule, namely biTYY-DPA, using first principles calculations that are consistent with previous experimental results of spin alignment with optical excitation. We find that the radical-triplet exchange interactions J_1 are very significantly enhanced (by approximately two orders of magnitude on average), which indicates a 'switching on' phenomenon for the two-qubit interaction by optical excitation. The time evolution of the reduced density matrix for the radicals indicates the possibility to create entanglement between the radicals through optical excitation and ISC on a spin coupler. We have also calculated the TREPR spectra based on the theory of open quantum systems, and the results are in qualitative agreement with previous experiments. The powder-averaged calculation has the potential to fit the experimental spectra quantitatively. Our calculations also indicate that the fidelity of the $\sqrt{\mathrm{SWAP}}$ quantum gate could be higher than 91%, which is an encouraging outcome for this type of design. These calculations will therefore facilitate the design of molecular networks for quantum computing. Our computational methodology, which integrates first-principles calculations and open-quantum-system spin dynamics simulations, can be further generalized to any radical-bearing molecules. The work presented here thus demonstrates a universal route to design molecular QC networks by integrating nanophotonic devices and suitable molecules, which would thus be made identifiable through machine learning screening[66,67]. The molecular quantum circuit blueprint proposed here not only represents progress toward the systematic scale-up of QC networks by orders of magnitude but also has great potential to achieve room-temperature quantum gate operation.

Acknowledgements

The authors gratefully acknowledge Prof. Hao Gong (National University of Singapore), Prof. Jing Liu (Technical Institute of Physics and Chemistry, Chinese Academy of Sciences & Tsinghua University), Prof. Zhenghong Lu (Yunnan University), Prof. Gabriel Aeppli, Prof. Sandrine Heutz, Prof. Chris Kay, Dr. Garvin Morley, the late Prof. Marshall Stoneham, and Dr. Marc Warner for helpful discussions. Thanks for the support of the Key Laboratory of Yunnan Provincial Higher Education Institutions for Optoelectronic Device Engineering at Yunnan University. The authors thank the National Natural Science Foundation of China (No. 62164006), Yunnan Fundamental Research Projects

(No.202201AS070008), Scientific Research Fund of Yunnan Education Department (No. 2023Y0886), Yunnan Key R&D Program Project Number: 202103AM140039, UK Research Councils Basic Technology Program (EP/F041349/1), UKRI Atomically Deterministic Doping and Readout For Semiconductor Solotronics Project (ADDRFSS, EP/M009564/1), the EU Horizon 2020 Marketplace Project (No. 760173), and UK STFC for funding.

Author details
[1]School of Physics and Astronomy, Center for Optoelectronics Engineering Research, Yunnan University, Kunming 650091, P. R. China. [2]School of Physical Science and Technology, Kunming University, Kunming, Yunnan Province, P. R. China. [3]Yunnan OceanDeepland Organic Optoelectronic Technology Ltd, 650214 Kunming, Yunnan Province, P. R. China. [4]UCL Department of Physics and Astronomy and London Centre for Nanotechnology, University College London, Gower Street, London WC1E 6BT, United Kingdom. [5]Department of Chemistry, Imperial College London, White City Campus, 80 Wood Lane, London W12 0BZ, United Kingdom. [6]UCL Institute for Materials Discovery, University College London, Malet Place, London WC1E 7JE, United Kingdom

Author contributions
W.W., A.J.F., N.M.H., T.Y.Z, and H.W. contributed to the concept of the paper. W.W., J.W.C., T.H.H., L.M., A.J.F. and N.M.H. performed the theoretical analysis. All the authors contributed to the drafting of the paper.

Data availability
All the computer code and data that support the findings of this study are available from the corresponding author upon reasonable request.

Conflict of interest
The authors declare no competing interests.

Publisher's note
Springer Nature remains neutral with regard to jurisdictional claims in published maps and institutional affiliations.

Received: 16 June 2023 Revised: 9 October 2023 Accepted: 17 October 2023
Published online: 01 December 2023

References

1. Alexeev, Y. et al. Quantum computer systems for scientific discovery. *PRX Quant.* **2**, 017001 (2021).
2. Warner, M. et al. Potential for spin-based information processing in a thin-film molecular semiconductor. *Nature* **503**, 504–508 (2013).
3. Atzori, M. et al. Room-temperature quantum coherence and rabi oscillations in vanadyl phthalocyanine: toward multifunctional molecular spin qubits. *J. Am. Chem. Soc.* **138**, 2154 (2016).
4. Moreno-Pineda, E., Godfrin, C., Balestro, F., Wernsdorfer, W. & Ruben, M. Molecular spin qudits for quantum algorithms. *Chem. Soc. Rev.* **47**, 501–513 (2018).
5. Atzori, M. & Sessoli, R. The second quantum revolution: role and challenges of molecular chemistry. *J Am. Chem. Soc.* **141**, 11339–11352 (2019).
6. Gaita-Ario, A., Luis, F., Hill, S. & Coronado, E. Molecular spins for quantum computation. *Nat. Commun.* **11**, 301–309 (2019).
7. Lunghi, A. & Sanvito, S. Computational design of magnetic molecules and their environment using quantum chemistry, machine learning and multiscale simulations. *Nat. Rev. Chem.* **6**, 761–781 (2022).
8. Carretta, S. et al. A perspective on scaling up quantum computation with molecular spins. *Appl. Phys. Lett.* **118**, 240501 (2021).
9. Coronado, E. Molecular magnetism: from chemical design to spin control in molecules, materials and devices. *Nat. Rev. Mater.* **5**, 87–104 (2020).
10. Moreno-Pineda, E. & Wernsdorfer, W. Measuring molecular magnets for quantum technologies. Nature Reviews. *Physics* **3**, 645–659 (2021).
11. Aravena, D. & Ruiz, E. Spin dynamics in single-molecule magnets and molecular qubits. *Dalton Trans.* **49**, 9916–9928 (2020).
12. Garlatti, E., Tesi, L., Lunghi, A., Atzori, M. & Carretta, S. Unveiling phonons in a molecular qubit with four-dimensional inelastic neutron scattering and density functional theory. *Nat. Commun.* **11**, 1751 (2020).
13. Laorenza, D. W. & Freedman, D. E. Could the Quantum Internet Be Comprised of Molecular Spins with Tunable Optical Interfaces? *J. Am. Chem. Soc.* **144**, 21810–21825 (2022).
14. Zhang, X. et al. Electron spin resonance of single iron phthalocyanine molecules and role of their non-localized spins in magnetic interactions. *Nat. Chem.* **14**, 59–65 (2022).
15. Auffeves, A. Quantum technologies need a quantum energy initiative. *PRX Quant.* **3**, 020101 (2022).
16. Filidou, V. et al. Ultrafast entangling gates between nuclear spins using photoexcited triplet states. *Nat. Phys.* **8**, 596–600 (2012).
17. Ma, L. et al. Triplet-radical spin entanglement: potential of molecular materials for high-temperature quantum information processing. *NPG Asia Mater.* **14**, 45 (2022).
18. Bayliss, S. L. et al. Optically addressable molecular spins for quantum information processing. *Science* **370**, 1309–1312 (2020).
19. Wasielewski, M. R. et al. Exploiting chemistry and molecular systems for quantum information science. *Nat. Rev. Chem.* **4**, 490–504 (2020).
20. Wu W., A quantum circuit architecture based on the integration of nano-photonic devices and two-dimensional molecular network. In Quantum Technology: Driving Commercialisation of an Enabling Science III (Vol. 12335, pp. 139–145). SPIE (2023).
21. Ratera, I. & Veciana, J. Playing with organic radicals as building blocks for functional molecular materials. *Chem. Soc. Rev.* **41**, 303–349 (2012).
22. Ji, L., Shi, J., Wei, J., Yu, T. & Huang, W. Air-Stable Organic Radicals: New-Generation Materials for Flexible Electronics? *Adv. Mater.* **32**, 1908015 (2020).
23. Lehmann, J., Gaita-Arino, A., Coronado, E. & Loss, D. Spin qubits with electrically gated polyoxometalate molecules. *Nat. Nanotechnol.* **2**, 312–317 (2007).
24. Ferrando-Soria, J. et al. A modular design of molecular qubits to implement universal quantum gates. *Nat. Commun.* **7**, 11377 (2016).
25. Atzori, M. et al. A two-qubit molecular architecture for electron-mediated nuclear quantum simulation. *Chem. Sci.* **9**, 6183–6192 (2018).
26. Ullah, A., Hu, Z., Cerdá, J., Aragó, J. & Gaita-Ariño, A. Electrical two-qubit gates within a pair of clock-qubit magnetic molecules. *npj Quant. Inform.* **8**, 133 (2022).
27. Dolphin D., The porphyrins (Academic Press, 1979).
28. Teki, Y., Miyamoto, S., Iimura, K., Nakatsuji, M. & Miura, Y. Intramolecular spin alignment utilizing the excited molecular field between the triplet (S = 1) excited state and the dangling stable radicals (S = 1/2) as studied by time-resolved electron spin resonance: observation of the excited quartet (S = 3/2) and quintet (S = 2) states on the purely organic π-conjugated spin systems. *J. Am. Chem. Soc.* **122**, 984–985 (2000).
29. Sato, O., Tao, J. & Zhang, Y. Z. Control of magnetic properties through external stimuli. *Angewandte Chemie Int. Edition* **46**, 2152–2187 (2007).
30. Ishii, K., Kubo, K., Sakurada, T., Komori, K. & Sakai, Y. Phthalocyanine-based fluorescence probes for detecting ascorbic acid: phthalocyaninatosilicon covalently linked to TEMPO radicals. *Chem. Commun.* **47**, 4932–4934 (2011).
31. Corvaja, C. et al. CIDEP of fullerene C60 biradical bisadducts by intramolecular triplet–triplet quenching: a novel spin polarization mechanism for biradicals. *Chem. Phys. Lett.* **330**, 287–292 (2000).
32. Franco, L. et al. TR-EPR of single and double spin labelled C60 derivatives: observation of quartet and quintet excited states in solution. *Mol. Phys.* **104**, 1543–1550 (2006).
33. Huai, P., Shimoi, Y. & Abe, S. Electronic control of spin alignment in π-conjugated molecular magnets. *Phys. Rev. Lett.* **90**, 207203 (2003).
34. Breuer H. P., & Petruccione F. *The theory of open quantum systems*. (Oxford University Press, USA, 2002).
35. Frisch M. J. et al. *Gaussian 09, revision A. 02*. (Gaussian Inc, Wallingford CT, 2009)
36. Noodleman, L. Valence bond description of antiferromagnetic coupling in transition metal dimers. *J. Chem. Phys.* **74**, 5737–5743 (1981).
37. Becke, A. Density-functional thermochemistry. III. The role of exact exchange. *J. Chem. Phys* **98**, 5648 (1993).
38. Illas, F. et al. Magnetic coupling in biradicals, binuclear complexes and wide-gap insulators: a survey of ab initio wave function and density functional theory approaches. *Theor. Chem. Acc.* **104**, 265–272 (2000).
39. Serri, M. et al. High-temperature antiferromagnetism in molecular semiconductor thin films and nanostructures. *Nat. Commun.* **5**, 3079 (2014).
40. Ivády, V. Longitudinal spin relaxation model applied to point-defect qubit systems. *Phys. Rev. B* **101**, 155203 (2020).
41. Blank, A. & Levanon, H. Triplet line shape simulation in continuous wave electron paramagnetic resonance experiments. *Conc. Magn. Resonance Part A: Educ. J.* **25**, 18–39 (2005).

42. Misra S. K. (Editor). *Multifrequency electron paramagnetic resonance: theory and applications*. (John Wiley & Sons, 2011).
43. Stoll, S. & Schweiger, A. Easy spin, a comprehensive software package for spectral simulation and analysis. *EPR. J. Magn. Reson.* **178**, 42–55 (2006).
44. Noda, H. et al. Critical role of intermediate electronic states for spin-flip processes in charge-transfer-type organic molecules with multiple donors and acceptors. *Nat. Mater.* **18**, 1084–1090 (2019).
45. Ovchinnikov, A. A. Multiplicity of the ground state of large alternant organic molecules with conjugated bonds: (Do Organic Ferromagnetics Exist?). *Theoret. Chim. Acta* **47**, 297–304 (1978).
46. Lieb, E. H. Two theorems on the Hubbard model. *Phys. Rev. Lett.* **62**, 1201 (1989).
47. Anderson, P. W. New approach to the theory of superexchange interactions. *Phys. Rev.* **115**, 2 (1959).
48. Boothroyd A. T. *Principles of neutron scattering from condensed matter*. (Oxford University Press, 2020).
49. Gao X. et al. Quantum computer aided design simulation and optimization of semiconductor quantum dots. *J. Appl. Phys*. **114**, (2013).
50. Niquet Y. M. et al. Challenges and perspectives in the modeling of spin qubits. In *2020 IEEE International Electron Devices Meeting* (IEDM) pp. 30–31 (IEEE, 2020).
51. Kyaw, T. H. et al. Quantum computer-aided design: digital quantum simulation of quantum processors. *Phys. Rev. Appl.* **16**, 044042 (2021).
52. Gibertini, M., Koperski, M., Morpurgo, A. F. & Novoselov, K. S. Magnetic 2D materials and heterostructures. *Nat. Nanotechnol.* **14**, 408–419 (2019).
53. Ferrari, A. C. et al. Science and technology roadmap for graphene, related two-dimensional crystals, and hybrid systems. *Nanoscale* **7**, 4598–4810 (2015).
54. Zhuang, X., Mai, Y., Wu, D., Zhang, F. & Feng, X. Two-dimensional soft nanomaterials: a fascinating world of materials. *Adv. Mater.* **27**, 403–427 (2015).
55. Kolb, H. C. & Sharpless, K. B. The growing impact of click chemistry on drug discovery. *Drug Discov. Today* **8**, 1128–1137 (2003).
56. Đorđević, T. et al. Entanglement transport and a nanophotonic interface for atoms in optical tweezers. *Science* **373**, 1511–1514 (2021).
57. Bogaerts, W. et al. Programmable photonic circuits. *Nature* **586**, 207–216 (2020).
58. Elshaari, A. W., Pernice, W., Srinivasan, K., Benson, O. & Zwiller, V. Hybrid integrated quantum photonic circuits. *Nat Photo.* **14**, 285–298 (2020).
59. Kern, J. et al. Nanoscale positioning of single-photon emitters in atomically thin Wse2. *Advanced materials* **28**, 7101–7105 (2016).
60. Ziegler, J. et al. Single-photon emitters in boron nitride nanococoons. *Nano Lett* **18**, 2683–2688 (2018).
61. Peng, L. et al. Creation of single-photon emitters in WSe2 monolayers using nanometer-sized gold tips. *Nano Lett.* **20**, 5866–5872 (2020).
62. Rosenberger, M. R. et al. Quantum calligraphy: writing single-photon emitters in a two-dimensional materials platform. *ACS Nano* **13**, 904–912 (2019).
63. Liu, S., Srinivasan, K. & Liu, J. Nanoscale positioning approaches for integrating single solid-state quantum emitters with photonic nanostructures. *Laser Photo. Rev.* **15**, 2100223 (2021).
64. Toninelli, C. et al. Single organic molecules for photonic quantum technologies. *Nat. Mater.* **20**, 1615–1628 (2021).
65. Benjamin, S. C. & Bose, S. Quantum computing with an always-on Heisenberg interaction. *Phys. Rev. Lett.* **90**, 247901 (2003).
66. Schleder, G. R. et al. DFT to machine learning: recent approaches to materials science–a review. *J. Phys.: Mater* **2**, 032001 (2019).
67. Butler, K. T., Davies, D. W., Cartwright, H., Isayev, O. & Walsh, A. Machine learning for molecular and materials science. *Nature* **559**, 547–555 (2018).